NIA grant: Ancillary to HCHS/SOL: MRI Measures of Cerebrovascular Injury and AD Atrophy in a Study of Latinos (RF1 AG054548, C DeCarli & H Gonzalez)

SOL-INCA-MRI Project Methods and Applications

Background

Magnetic Resonance Imaging (MRI) is a powerful tool used to assess brain differences associated with aging and the presence of various diseases.

The SOL-INCA-MRI project was designed to advance understanding of the prevalence, cognitive consequences, and potential differences in genetic architecture of vascular brain and degenerative injury within the community based and representative Latino population of HCHS/SOL.

This project is a unique opportunity to study a large and representative group of Latinos and will extend current scientific knowledge by contributing to a growing and increasingly diverse MRI and genetics database from other community based studies such as the Framingham Heart Study (FHS), Atherosclerosis Risk in Communities Study, Cardiovascular Health Study, Chicago Healthy Aging Project (CHAP), Washington Heights Inwood Columbia Aging Project (WHICAP) and the Northern Manhattan Stroke Study (NOMAS) that have similar imaging variables. Dr. DeCarli and the IDeA laboratory have contributed MRI data to these studies. Fully understanding the public health consequences of vascular risk factors as well the genetic influences on brain health and MCI or AD requires large collaborative study groups. Until now, these groups has been limited to data from Caribbean Latinos (e.g. WHICAP and NOMAS), despite the fact that Mexican Americans constitute the majority of Latino Americans[1].

Aim

The goal of this paper is to describe MRI data obtained under RF1 AG054548, "MRI Measures of Cerebrovascular Injury and AD Atrophy in a Study of Latinos" (SOL-INCA-MRI) and give general use guidance to the analysis and interpretation of these data.

Data Sharing

The co-principal investigators of this study encourage vigorous use of these data in accordance with HCHS/SOL policies and procedures as outlined in the public information section of the HCHS/SOL website https://sites.cscc.unc.edu/hchs/publications-pub. Given the somewhat complex nature of these datasets, we strongly recommend collaboration with members of the SOL-INCA-MRI team as you develop your publication proposal.

Charles DeCarli, MD, cdecarli@ucdavis.edu, Contact PI.
Hector Gonzalez, PhD, hectorgonzalez@health.ucsd.edu, Co-PI
Myriam Fornage, PhD, Myriam.Fornage@uth.tmc.edu, Co-investigator and genetic epidemiologist
Wassim Tarraf, PhD, ai2483@wayne.edu, Co-investigator and biostatistician
Pauline Maillard, PhD, pmaillar@ucdavis.edu, Co-investigator and imaging scientist

Data

Brief description of the HCHS/SOL parent study

The Hispanic Community Health Study (HCHS)/Study of Latinos (SOL) is a multicenter, community-based cohort study of Hispanic/Latino adults in the United States. A diverse participant sample is required that is both representative of the target population and likely to remain engaged throughout follow-up. The study design calls for recruitment and follow-up of a cohort of 16,000 Hispanics/Latinos 18–74 years of age, with 62.5% (10,000) over 44 years of age and adequate subgroup sample sizes to support inference by Hispanic/Latino background. Participants are recruited in community areas surrounding four field centers in the Bronx, Chicago, Miami, and San Diego. A two-stage area probability sample of households is selected with stratification and oversampling incorporated at each stage to provide a broadly diverse sample, offer efficiencies in field operations, and ensure that the target age distribution is obtained. Embedding probability sampling within this traditional, multisite cohort study design enables competing research objectives to be met. However, the use of probability sampling requires developing solutions to some unique challenges in both sample selection and recruitment[2].

Brief description of SOL-INCA

The Study of Latinos-Investigation of Neurocognitive Aging (SOL-INCA) is an ancillary study of HCHS/SOL. The purpose of SOL-INCA (years 2016-2018) is to assess neurocognitive function and change among participants ages 45-74 who underwent cognitive assessment at time of Visit 1 (n=6,377). The research framework of the SOL-INCA has been published.[3]

Brief description of SOL-INCA-MRI

MRI Measures of Cerebrovascular Injury and Alzheimer's disease Atrophy in a Study of Latinos (RF1 AG054548; AKA SOL-INCA-MRI)" in collaboration with SOL-INCA was designed to identify biological underpinnings of normal cognitive aging, MCI and Alzheimer's disease and related dementias (ADRD) in a representative subgroup of the Hispanic Community Health Study/Study of Latinos (HCHS/SOL) 64 ± 7 years of age on average. The primary aims of SOL-INCA-MRI were to examine 1) the relationship between prevalent vascular risk factors and brain structure throughout the age continuum; 2) the impact of these measures on cognition; and 3) genetic influences on select brain measures. Given emphasis on aging for Aim 1, SOL-INCA-MRI included a random subgroup of younger participants. The figure summarizes the final cohort configuration.

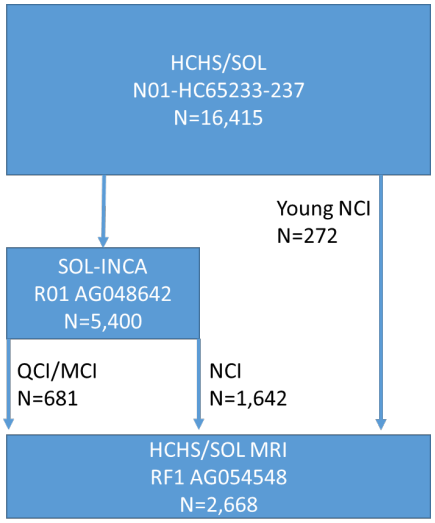

Description of MRI Methods

The MRI data acquired for SOL-INCA-MRI includes: 1) Structural MRI measures, 2) Diffusion Tensor Imaging (DTI) measures, 3) Infarctions (MR Infarcts) and 4) Cerebral Microbleeds (CMB).

The specific data elements involved quantitative and qualitative analyses that will be described under each database heading.

Structural Brain Imaging Measures

inca_mri_struc_inv3

1) *Image Segmentation:* Structural image analysis begins with automatic removal of non-brain elements[4] (with human correction) from the 3D T1 image volume and segmentation of the image into 4 tissue classes (gray, white, cerebral spinal fluid (CSF)[5, 6] and white matter hyperintensities (WMH)[7, 8]) as shown here.

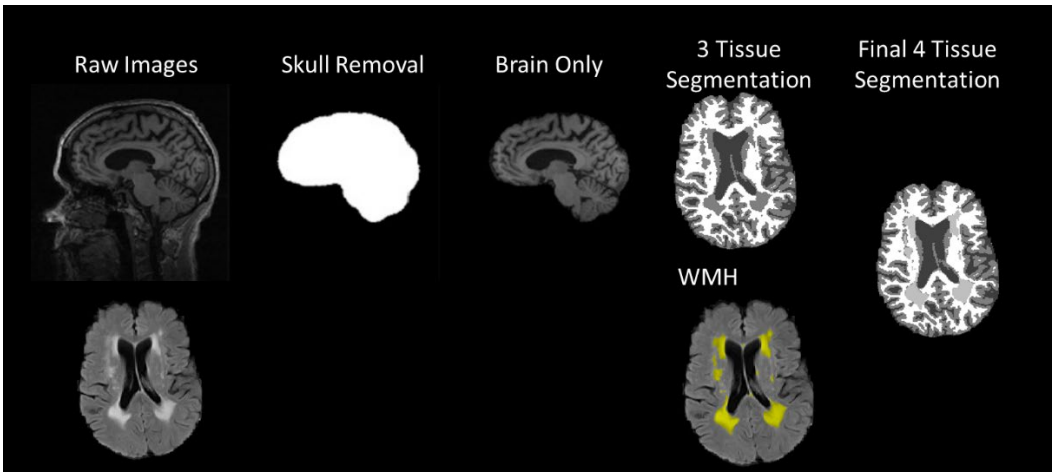

2) *Tissue Volume Quantitation*: The segmented image is further divided into general and regional measures.
   - **a.** Global Measures which include:
     - **i.** Cranial volume (Total Cranial Volume)
     - **ii.** Brain measure (Total Cerebral Brain Volume)
     - **iii.** Gray matter measure (Total Cerebral Gray Matter Volume)
     - **iv.** White matter measure (Total Cerebral White Matter Volume)
     - **v.** Total cranial CSF (Total Cerebral Spinal Fluid Volume)
     - **vi.** Total White Matter Hyperintensity Volume (WMH).
   - **b.** Total Cerebral Gray Matter + Total White Matter Volume = Total Cerebral Brain Volume.
   - **c.** Total Cerebral Brain Volume + Total Cerebral Spinal Fluid Volume = Total Cranial Volume.

     Note: Total Cerebral Gray Matter Volume may be contaminated by WMH. Subtracting WMH volume will lead to a more accurate measure.

   - d. Regional Measures:
     - i. Cortical Measures: The cortical gray matter is further subdivided into 4 lobes (Frontal, Parietal, Temporal and Occipital) as well 101 smaller regions as defined by the "Desikan-Killiany-Tourville" (DKT) atlas[9].
     - ii. Hippocampal Measures. We also quantify the entire hippocampal volume based on internationally recognized guidelines[10, 11].
     - iii. CSF Measures: These include the right, left and total lateral ventricle volumes as well as the 3rd ventricle volume.

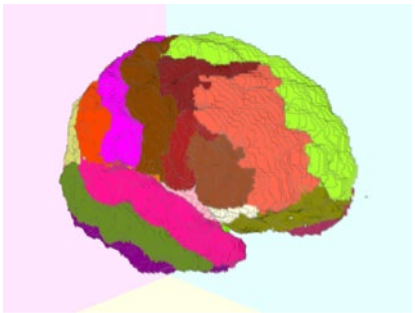

3) *Head Size Correction*: Total Cranial Volume (TCV) is highly associated with brain growth during normal development [12], whereas aging or disease-related brain-volume decrease does not alter TCV. Thus, adult TCV is a stable valid measure for maximal attained brain size, widely used as a proxy for brain reserve[13, 14], and is an important predictor of cognition in old age[15]. In addition, there is substantial sexual dimorphism in TCV[16]. Consequently, correction for head size (TCV) is a standard approach to analysis of structural brain regions. For SOL-INCA-MRI, we use residuals of regression by TCV as the major variables for analyses.

4) *Cortical Thickness*: This measure is calculated using the DiReCT (Diffeomorphic Registration-based Cortical Thickness) method[17]. Average regional thickness measures, in millimeters (mm) is available for each of the lobar and regional measures from the DKT atlas.

5) *Mean White Matter Diffusion Tensor Imaging (DTI)*: inca_mri_dti_inv3
This measure is used primarily for assessment of white matter integrity. Consequently, for this project, we report only white matter measures. DTI is a more complicated method, and we recommend that use of these variables be done in consultation with one of the SOL-INCA-MRI investigators, particularly Dr. Pauline Maillard. In this dataset, we report 3 global white matter DTI measures: Mean Fractional Anisotropy (FA), Mean Free Water (FW) and Peak Skeletonized Mean Diffusivity (PSMD). FA describes the alignment and integrity of white matter tracks and varies from 0 (complete isotropy) to 1 (complete anisotropy). FA is reduced in the setting of injury. FW and PSMD are measures of fluid movement within white matter and are increased in the setting of injury.
6) *Tract Specific White Matter Diffusion Tensor Imaging (fDTI)*: inca_mri_fdti_inv3
FA and FW are also calculated for specific white matter tracts as summarized by the table below.

ID	FIBERNAME	DATE	FW_TRACT	FA_TRACT	FIBER NUMBER
0	Middle_cerebellar_peduncle	01/01/2001	0.171325	0.542748	1
0	Pontine_crossing_tract_(a_part_of_MCP)	01/01/2001	0.105837	0.472129	2
0	Genu_of_corpus_callosum	01/01/2001	0.300821	0.748317	3
0	Body_of_corpus_callosum	01/01/2001	0.292671	0.734395	4
0	Splenium_of_corpus_callosum	01/01/2001	0.20398	0.77378	5
0	Fornix_(column_and_body_of_fornix)	01/01/2001	0.68863	0.687255	6
0	Corticospinal_tract	01/01/2001	0.152367	0.591289	7
0	Medial_lemniscus	01/01/2001	0.155248	0.5866	8
0	Inferior_cerebellar_peduncle	01/01/2001	0.18178	0.552313	9
0	Superior_cerebellar_peduncle	01/01/2001	0.319266	0.668984	10
0	Cerebral_peduncle	01/01/2001	0.190191	0.692658	11
0	Anterior_limb_of_internal_capsule	01/01/2001	0.120495	0.567504	12
0	Posterior_limb_of_internal_capsule	01/01/2001	0.113413	0.62566	13
0	Retrolenticular_part_of_internal_capsule	01/01/2001	0.167355	0.611783	14
0	Anterior_corona_radiata	01/01/2001	0.185681	0.478616	15
0	Superior_corona_radiata	01/01/2001	0.128765	0.500787	16
0	Posterior_corona_radiata	01/01/2001	0.186046	0.537678	17
0	Posterior_thalamic_radiation_(include_optic_radiation)	01/01/2001	0.22942	0.645876	18

0	Sagittal_stratum_ (include_inferior_longitidinal_fasciculus_and_inferior_ fronto-occipital_fasciculus)	01/01/2001	0.260513	0.603591	19
0	External_capsule	01/01/2001	0.175993	0.472384	20
0	Cingulum_(cingulate_gyrus)	01/01/2001	0.170183	0.524164	21
0	Cingulum_(hippocampus)	01/01/2001	0.218011	0.436223	22
0	Fornix_(cres)_/_Stria_terminalis	01/01/2001	0.270493	0.61263	23
0	Superior_longitudinal_fasciculus	01/01/2001	0.152441	0.494753	24
0	Superior_fronto-occipital_fasciculus_(could_be_a_part_of_ anterior_internal_capsule)	01/01/2001	0.115825	0.451555	25
0	Uncinate_fasciculus	01/01/2001	0.206492	0.485613	26
0	Tapetum	01/01/2001	0.506391	0.673017	27

7) *PSMD*: is a measure of diffusivity within a select area of the white matter as shown here:

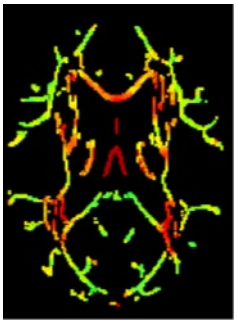

All 3 measures are included in the inca_mri_dti_inv3 file.
In addition, mean FA and FW values for each of 27 white matter tracks from the Johns Hopkins University (Mori) atlas[18] are included in a separate file: inca_mri_fdti_inv3.

Magnetic Resonance Infarctions

inca_mri_stroke_inv3

Clinically silent cerebral infarction is a common finding amongst older individuals within a community cohort[16] and share the same risk factors and outcomes as clinically apparent stroke[19, 20]. For this study, the presence of MRI infarction was determined from the size, location, and imaging characteristics of the lesion. Signal void, best seen on T2 weighted images, was interpreted to indicate a vessel. Only lesions 3mm or larger qualified for consideration as cerebral infarcts. Other necessary imaging characteristics included: 1) CSF signal characteristics on the subtraction image and 2) if the infarct was in the basal ganglia area, distinct separation from the circle of Willis vessels. These data are included in the file inca_mri_stroke_inv3 where infarctions are identified as present or absent. If present, then the location, type and number of infarcts are identified along with the image coordinates in XYZ format as shown in the example below.

ANALYZER	NAME	MRI DATE	ANALYZE DATE	SIDE	SIZE	CVA NUMBER	CVA LOCATION	CVA TYPE	XYZ
cd	xxx.img	01/01/2000	01/02/2000	LEFT	MICRO	1	BASAL GANGLIA	THROMBOSIS	236-475-179

Cerebral Microbleeds

Inca_mri_cmb_inv3

Small foci of chronic blood products in normal (or near normal) brain tissue, designated as cerebral microbleeds (CMB), have been an increasingly recognized entity since the widespread application of magnetic resonance imaging (MRI) techniques tailored to detect magnetic susceptibility[21]. CMB can occur with normal aging, cerebrovascular diseases such as hypertension, and dementia due to Alzheimer's disease where CMB may represent the presence of cerebral amyloid angiopathy[22-24].

CMB are defined as rounded, generally < 1 cm signal loss on T2* weighted imaging, particularly gradient recalled echo (GRE) imaging. The signal loss, termed "magnetic susceptibility" is believed to result from local magnetic field distortions due to the presence of small amounts of hemosiderin (an iron containing blood byproduct) in the brain. Magnetic susceptibility, however, is not specific to hemosiderin, but may occur in the presence of other minerals such as calcium. In addition, CMB need to be distinguished from blood vessels as flowing blood also causes similar field distortion, areas near bone where the air bone transition can also cause signal loss and angiomas, which are generally larger[21].

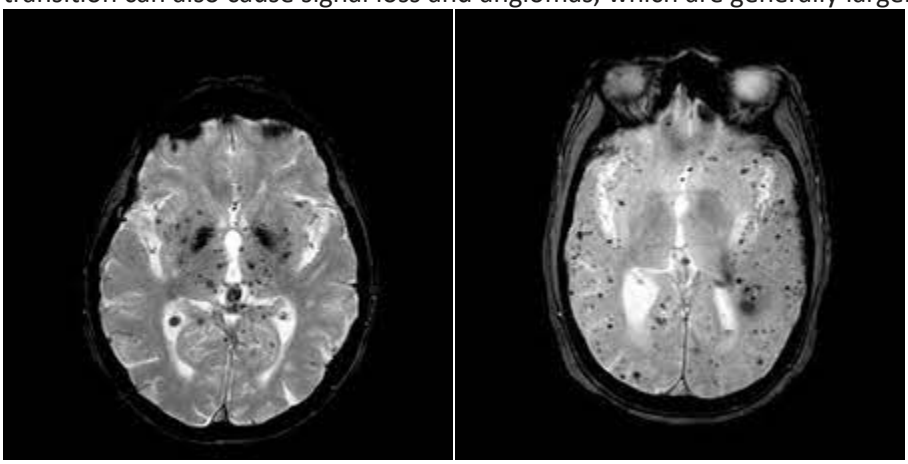

To date, most use operator guided methods to detect CMB[21], although automated methods show future promise. The general approach is to identify the presence or absence of any CMB, localize and count (if possible) the number at each location. This approach is based on the hypothesis that the pathophysiology of CMB differ by location with CMB in "deep" locations (left image) more commonly due to cerebrovascular disease and "lobar" locations (right image) due mostly to cerebral amyloid angiopathy[22]. Because these are operator defined, reliability is important[21].
CMB location in the brain was classified into subgroups based on assumed pathophysiology (cerebral amyloid angiopathy [CAA] and hypertensive vasculopathy). These subgroups are separately recorded as present (1) or absent (0):

1) Any CMB: includes participants with CMB in any brain location, deep, lobar, and/or both,
2) Lobar only: includes participants with CMB in the cortex and subcortical white matter in cerebral hemisphere.
3) Deep only: includes participants with CMB in deep regions: basal ganglia, thalamus, white matter of the internal and external capsules, brainstem, and cerebellum.
4) Mixed: includes participants who have CMB in both deep and lobar regions.
5) Deep and mixed: includes participants who had CMB in deep regions in addition to participants with CMB in mixed location (i.e. deep only + mixed)
6) Lobar and mixed: included participants who had CMB in lobar regions in addition to participants with CMB in mixed location (i.e. lobar only + mixed).

Finally, the number of CMB for each participant in the lobar only, deep only, or mixed categories is also counted and recorded (see below for example).

Subject	any CMB	lobar CMB	# lobar	mixed CMB	# mixed	deep CMB	# deep	deep + mixed	lobar + mixed
xyz	1	0	27	1	45	0	18	1	1

Suggested Approaches to Analyses of Imaging Data

1. Center-specific adjustments. HCHS/SOL guidelines recommend adjusting for Center-specific effects. When using MRI data, we recommend use of the MANUFACTURERSMODELNAME instead. This variable adjusts for both Center-specific effects as well as changes in MRI machine within a center.
2. Machine specific Adjustments for DTI. The variable BVALUES in the DTI files is a string indicator of DTI acquisition sequence. This alphanumeric variable specifies number of directions "_" gradient b value "/" number of b0 acquisitions n_b0. For example, 60_b1000/6_b0/ is 60 directions obtained at a gradient of 1000 with 6 images at b=0. Work by our group finds that adjustment by number of directions is most important.
3. Given the selection criteria that emphasized enriching participants with cognitive impairment, we advise against making population inferences based on sample weights as they do not account for degree of cognitive impairment.

How to Cite These Methods

Removal of Non-brain tissues: The skull is removed using a convolutional neural net method[4] followed by human quality control to provide generally minor cleanup if needed. Structural MRI brain images are then nonlinearly registered performed by a cubic B-spline deformation [25] to a minimal deformation template (MDT) synthetic brain image[26] adapted for age range of 60 and above.

Image Intensity Inhomogeneity Correction: B1 field inhomogeneity is a common problem that limits the precision of image segmentation. We utilize a template-based iterative method for correcting field inhomogeneity bias[5]. At each algorithm iteration, the update of a B-spline deformation between an unbiased template image and the subject image is interleaved with estimation of a bias field based on the current template-to-image alignment. The bias field is modeled using a spatially smooth thin-plate spline interpolation based on ratios of local image patch intensity means between the deformed template and subject images. This is used to iteratively correct subject image intensities which are then used to improve the template-to-image deformation.

Gray, White and CSF Measurement: Our segmentation algorithm is based on an Expectation-Maximization (EM) algorithm that iteratively refines its segmentation estimates to produce outputs that are most consistent with the input intensities from the native-space T1 images along with a model of image smoothness [6, 27]. Like all EM algorithms, the system must be initialized with a reasonable estimate. We produce this initial estimate from the template-space warps of previously segmented images; because locations of WM/GM/CSF tissues are known in the template space, transforming these masks back to each image's native space produces rough estimate 3-tissue segmentations. We then calculate the mean and standard deviation of the image intensities in locations labeled as each tissue type. These values then form the initial parameters for a Gaussian model of image intensity for each class. At each iteration, the algorithm uses a Gaussian model of T1-weighted image intensity for each tissue class, in order to produce a segmentation. In the first iteration, these models are estimated as described above. The segmentation yielded by these appearance models alone is then refined using a Markov Random Field (MRF) model, a computational statistical method that efficiently produces a label map consistent with both the input intensities and image smoothness statistics. Inference in the MRF is computed using an adaptive priors model[6]. This refined segmentation from the MRF is then used to compute new Gaussian intensity models for each tissue class, and the algorithm repeats, iteratively switching between calculating Gaussian appearance models and MRF-based segmentation, until convergence. The MRF-based segmentation at the final iteration is used as the final output segmentation.

White Matter Hyperintensity: WMH is performed on a combination of FLAIR and 3D T1 images using a modified Bayesian probability structure based on a previously published method of histogram fitting [28]. Prior probability maps for WMH were created from more than 700 individuals with semi-automatic detection of WMH followed by manual editing. Likelihood estimates of the native image are calculated through histogram segmentation and thresholding. All segmentation is initially performed in standard space resulting in probability likelihood values of WMH at each voxel in the white matter. These probabilities are then thresholded at 3.5 sd above the mean to create a binary WMH mask. Further segmentation is based on a modified Bayesian approach that combines image likelihood estimates, spatial priors, and tissue class constraints. The segmented WMH masks are then back transformed on to native space for tissue volume calculation. Reliability of this method is well-established[29]

Automatic Hippocampal Segmentation: MRI-derived hippocampal volumetry has been a widely used biomarker in AD to improve early diagnosis[30], enrich subject selection[31], and monitor

treatment efficacy[32, 33]. To address this need, the EADC-ADNI Working Group established a Delphi panel to determine the optimum protocol[10], selected orientation parameters[34] and developed the final, rigorously tested protocol along with making publicly available labels from over 100 ADNI subjects[11]. Our hippocampal segmentation method employs a standard atlas based diffeomorphic approach[35] with the minor modification of label refinement. We further modified this approach to include the EADC-ADNI harmonized hippocampal masks to assure standardization across cohorts. Therefore we have adopted the following approach: 1) Subject image pre-processing with extraction of intracranial cavity, non-uniformity correction, tissue classification as discussed above; 2) Atlas Registration of all EADC-ADNI hippocampal masks[10, 11, 30, 36, 37] to each subject; 3) Atlas Fusion utilizing MALF [38, 39]; and 4) Intensity-based label refinement.

ROI-based Analysis: Software developed by the IDeA laboratory allows the creation of any set of user-defined ROIs or utilization of published ROIs. The lab provides multiple sets of predefined regions of interest including lobar volumes, the Desikan-Killiany-Tourville Atlas[9]. Regional measures are calculated by back transformation of the atlas into segmented image native space. A voting scheme is used to assure precise labelling of each region after interpolation of the atlas into native space.

Cortical Thickness: We utilize a registration based method based on Das et al.[17, 40] which consists of the following steps: an initial probabilistic segmentation of GM, WM and CSF after intensity inhomogeneity correction[5] using our segmentation methods [6]. From the three probability maps, a three-label image is formed by picking the tissue type with the highest probability at each voxel. A greedy diffeomorphic registration algorithm is then used to expand the WM segment, to match the GM + WM segment or until a maximum of 6 mm displacement is reached. For each boundary voxel on the GM/WM boundary, the thickness is calculated as the distance moved under the registration transformation, and this thickness value is then propagated across the GM mask.

Infarcts: The presence of MRI infarction was determined from the size, location, and imaging characteristics of the lesion. The image analysis system allowed for superimposition of the subtraction image, the proton density image and the T2 weighted image at three times magnified view to assist in interpretation of lesion characteristics. Signal void, best seen on the T2 weighted image was interpreted to indicate a vessel. Only lesions 3mm or larger qualified for consideration as cerebral infarcts. Other necessary imaging characteristics included: 1) CSF density on the subtraction image and 2) If the stroke was in the basal ganglia area, distinct separation from the circle of Willis vessels. Kappa values for agreement amongst the three raters are generally good and range from 0.73 to 0.90. The Kappa value for 2 raters of SOL-INCA-MRI = 0.87.

Free Water and Fractional Anisotropy: The model considers two co-existing compartments per voxel: one compartment is a free-water compartment, which models isotropic diffusion with a diffusion coefficient of water at body temperature (37 °C) fixed to 3 × 10−3 mm2/s[41]. The free-water fraction is expected to predominantly highlight water molecules in the extracellular space. The second compartment is the tissue compartment, which accounts for all other molecules, i.e., all intra- and extracellular molecules that are hindered or restricted by tissue membranes[42]. The method contains the following steps: 1) DTI dataset are preprocessed using FSL software tools[43] including correction for eddy current-induced distortions and participant's head movements, 2) the tissue compartment is modeled by a diffusion tensor characterizing the “tissue” molecules, as well as the fractional volume of the free-water compartment in each voxel, resulting in the FW fraction map, 3) the individual FA map obtained from DTIFIT is linearly and non-linearly registered to the standard FSL FA template space (FMRIB 1-mm FA template)

using linear and nonlinear transformations[43], 4) the resulting transformation parameters are applied to the FW and FW- corrected FA maps, 5) a WM mask is defined by thresholding the FSL FA template at a value of 0.3 to reduce cerebrospinal fluid (CSF) partial volume contamination[44], 6) overall measures of mean FW and mean FA are computed by superimposing the WM mask onto the individual coregistered FW and FA maps and averaging values within these WM voxels.

Peak Width of Skeletonized Mean Diffusivity: The method follows the PSMD procedure previously described[45]. Briefly, it requires FA, MD, RD, and AD maps. The script procedure includes the following steps: 1) DTI dataset are preprocessed using FSL software tools[43] including correction for eddy current-induced distortions and participant's head movements, (2) the brain is masked using the BET tool, 3) fractional anisotropy (FA), mean diffusivity (MD), axial diffusivity (AD), and radial diffusivity (RD) maps are generated using DTIFIT[43], 4) the FA volume is linearly and non-linearly registered to the standard space FMRIB FSL 1-mm FA template; 5) a white matter skeleton is created using the standard Tract-based Spatial Statistics (TBSS)[46] pipeline available in FSL; 6) subject's FA data is then projected onto the skeleton, which is derived from the standard space template thresholded at an lower-bound FA value of 0.2 to exclude predominantly non-white matter voxels[44]; 7) MD volume is projected onto the mean FA skeleton using the FA-derived projection parameters and further thresholded with a template skeleton mask to reduce CSF partial volume contamination; 8) PSMD is calculated as the difference between the 95th and 5th percentiles of the voxel-based MD values within the subject's MD skeleton.

Applied use of these DTI methods for reliability and biological validation are cited by these references[29, 47, 48]

References

1. Bureau UC. 2010 Census, Summary File 1. Washington, D.C.: US Census Bureau, 2010.
2. Lavange LM, Kalsbeek WD, Sorlie PD, et al. Sample design and cohort selection in the Hispanic Community Health Study/Study of Latinos. Ann Epidemiol 2010;20:642-649.
3. González HM, Tarraf W, Fornage M, et al. A research framework for cognitive aging and Alzheimer's disease among diverse US Latinos: Design and implementation of the Hispanic Community Health Study/Study of Latinos—Investigation of Neurocognitive Aging (SOL-INCA). Alzheimer's & Dementia 2019;15:1624-1632.
4. Fletcher E, DeCarli C, Fan AP, Knaack A. Convolutional Neural Net Learning Can Achieve Production-Level Brain Segmentation in Structural Magnetic Resonance Imaging. Front Neurosci 2021;15:683426.
5. Fletcher E, Carmichael O, Decarli C. MRI non-uniformity correction through interleaved bias estimation and B-spline deformation with a template. Conf Proc IEEE Eng Med Biol Soc 2012;2012:106-109.
6. Fletcher E, Singh B, Harvey D, Carmichael O, Decarli C. Adaptive image segmentation for robust measurement of longitudinal brain tissue change. Conf Proc IEEE Eng Med Biol Soc 2012;2012:5319-5322.
7. DeCarli C, Fletcher E, Ramey V, Harvey D, Jagust WJ. Anatomical mapping of white matter hyperintensities (WMH): exploring the relationships between periventricular WMH, deep WMH, and total WMH burden. Stroke 2005;36:50-55.
8. Maillard P, Fletcher E, Harvey D, et al. White matter hyperintensity penumbra. Stroke 2011;42:1917-1922.

9. Klein A, Tourville J. 101 labeled brain images and a consistent human cortical labeling protocol. Front Neurosci 2012;6:171.
10. Boccardi M, Bocchetta M, Apostolova LG, et al. Delphi definition of the EADC-ADNI Harmonized Protocol for hippocampal segmentation on magnetic resonance. Alzheimers Dement 2014.
11. Bocchetta M, Boccardi M, Ganzola R, et al. Harmonized benchmark labels of the hippocampus on magnetic resonance: The EADC-ADNI project. Alzheimers Dement 2014.
12. Mori E, Hirono N, Yamashita H, et al. Premorbid brain size as a determinant of reserve capacity against intellectual decline in Alzheimer's disease. Am J Psychiatry 1997;154:18-24.
13. Farias ST, Mungas D, Reed B, et al. Maximal brain size remains an important predictor of cognition in old age, independent of current brain pathology. Neurobiol Aging 2011.
14. Gale CR, Walton S, Martyn CN. Foetal and postnatal head growth and risk of cognitive decline in old age. Brain 2003;126:2273-2278.
15. van Loenhoud AC, Groot C, Vogel JW, van der Flier WM, Ossenkoppele R. Is intracranial volume a suitable proxy for brain reserve? Alzheimers Res Ther 2018;10:91.
16. DeCarli C, Massaro J, Harvey D, et al. Measures of brain morphology and infarction in the framingham heart study: establishing what is normal. Neurobiol Aging 2005;26:491-510.
17. Tustison NJ, Cook PA, Klein A, et al. Large-scale evaluation of ANTs and FreeSurfer cortical thickness measurements. Neuroimage 2014;99:166-179.
18. Mori S, Kaufmann WE, Davatzikos C, et al. Imaging cortical association tracts in the human brain using diffusion-tensor-based axonal tracking. Magn Reson Med 2002;47:215-223.
19. Das RR, Seshadri S, Beiser AS, et al. Prevalence and correlates of silent cerebral infarcts in the Framingham offspring study. Stroke 2008;39:2929-2935.
20. Debette S, Beiser A, Decarli C, et al. Association of MRI Markers of Vascular Brain Injury With Incident Stroke, Mild Cognitive Impairment, Dementia, and Mortality. The Framingham Offspring Study. Stroke 2010.
21. Greenberg SM, Vernooij MW, Cordonnier C, et al. Cerebral microbleeds: a guide to detection and interpretation. Lancet Neurol 2009;8:165-174.
22. Romero JR, Preis SR, Beiser A, et al. Risk factors, stroke prevention treatments, and prevalence of cerebral microbleeds in the Framingham Heart Study. Stroke 2014;45:1492-1494.
23. Romero JR, Beiser A, Himali JJ, Shoamanesh A, DeCarli C, Seshadri S. Cerebral microbleeds and risk of incident dementia: the Framingham Heart Study. Neurobiol Aging 2017;54:94-99.
24. Romero JR, Preis SR, Beiser A, et al. Cerebral Microbleeds as Predictors of Mortality: The Framingham Heart Study. Stroke 2017;48:781-783.
25. Rueckert D, Aljabar P, Heckemann RA, Hajnal JV, Hammers A. Diffeomorphic registration using B-splines. Med Image Comput Comput Assist Interv 2006;9:702-709.
26. Kochunov P, Lancaster JL, Thompson P, et al. Regional spatial normalization: toward an optimal target. J Comput Assist Tomogr 2001;25:805-816.
27. Rajapakse JC, Giedd JN, DeCarli C, et al. A technique for single-channel MR brain tissue segmentation: application to a pediatric sample. Magnetic Resonance Imaging 1996;14:1053-1065.
28. DeCarli C, Miller BL, Swan GE, et al. Predictors of brain morphology for the men of the NHLBI twin study. Stroke 1999;30:529-536.
29. Maillard P, Lu H, Arfanakis K, et al. Instrumental validation of free water, peak-width of skeletonized mean diffusivity, and white matter hyperintensities: MarkVCID neuroimaging kits. Alzheimers Dement (Amst) 2022;14:e12261.
30. Frisoni GB, Bocchetta M, Chetelat G, et al. Imaging markers for Alzheimer disease: which vs how. Neurology 2013;81:487-500.

31. Lorenzi M, Donohue M, Paternico D, et al. Enrichment through biomarkers in clinical trials of Alzheimer's drugs in patients with mild cognitive impairment. Neurobiol Aging 2010;31:1443-1451, 1451 e1441.
32. Hampel H, Frank R, Broich K, et al. Biomarkers for Alzheimer's disease: academic, industry and regulatory perspectives. Nat Rev Drug Discov 2010;9:560-574.
33. Hampel H, Wilcock G, Andrieu S, et al. Biomarkers for Alzheimer's disease therapeutic trials. Prog Neurobiol 2011;95:579-593.
34. Boccardi M, Bocchetta M, Apostolova LG, et al. Establishing magnetic resonance images orientation for the EADC-ADNI manual hippocampal segmentation protocol. J Neuroimaging 2014;24:509-514.
35. Vercauteren T, Pennec X, Perchant A, Ayache N. Non-parametric diffeomorphic image registration with the demons algorithm. Med Image Comput Comput Assist Interv 2007;10:319-326.
36. Boccardi M, Bocchetta M, Ganzola R, et al. Operationalizing protocol differences for EADC-ADNI manual hippocampal segmentation. Alzheimers Dement 2013.
37. Frisoni GB, Jack CR. HarP: The EADC-ADNI Harmonized Protocol for manual hippocampal segmentation. A standard of reference from a global working group. Alzheimers Dement 2015;11:107-110.
38. Wang H, Suh JW, Das SR, Pluta J, Craige C, Yushkevich PA. Multi-Atlas Segmentation with Joint Label Fusion. IEEE Trans Pattern Anal Mach Intell 2012.
39. Wang H, Yushkevich PA. Dependency Prior for Multi-Atlas Label Fusion. Proc IEEE Int Symp Biomed Imaging 2012;2012:892-895.
40. Das SR, Avants BB, Grossman M, Gee JC. Registration based cortical thickness measurement. Neuroimage 2009;45:867-879.
41. Pierpaoli C, Basser PJ. Toward a quantitative assessment of diffusion anisotropy. Magn Reson Med 1996;36:893-906.
42. Pasternak O, Sochen N, Gur Y, Intrator N, Assaf Y. Free water elimination and mapping from diffusion MRI. Magnetic resonance in medicine : official journal of the Society of Magnetic Resonance in Medicine / Society of Magnetic Resonance in Medicine 2009;62:717-730.
43. Jenkinson M, Beckmann CF, Behrens TE, Woolrich MW, Smith SM. Fsl. Neuroimage 2012;62:782-790.
44. Smith SM, Kindlmann G, S. J. Cross-Subject Comparison of Local Diffusion MRI Parameters. Diffusion MRI (Second Edition). San Diego: Academic Press, 2014: 209-239.
45. Baykara E, Gesierich B, Adam R, et al. A Novel Imaging Marker for Small Vessel Disease Based on Skeletonization of White Matter Tracts and Diffusion Histograms. Ann Neurol 2016;80:581-592.
46. Smith SM, Jenkinson M, Johansen-Berg H, et al. Tract-based spatial statistics: voxelwise analysis of multi-subject diffusion data. Neuroimage 2006;31:1487-1505.
47. Maillard P, Fletcher E, Singh B, et al. Cerebral white matter free water: A sensitive biomarker of cognition and function. Neurology 2019;92:e2221-e2231.
48. Maillard P, Hillmer LJ, Lu H, et al. MRI free water as a biomarker for cognitive performance: Validation in the MarkVCID consortium. Alzheimers Dement (Amst) 2022;14:e12362.